SCIENTIFIC REPORTS

OPEN

Molecular alignment in degenerated dissociation channels in strong laser fields

Received: 6 December 2016
Accepted: 19 April 2017
Published online: 31 May 2017

Wei Lai, Alan Heins & Chunlei Guo

In this work, we study strong-field molecular alignment in, for the first time, degenerated channels following the same charged states of molecules. By measuring the angular distribution of dissociation fragments from two degenerated $N^+ + N^+$ channels of N_2, we observe an opposite angular distribution development in these two channels, one expanding and one contracting, when the laser intensity increases. Our further study shows that the expanding channel comes from a nonsequential transition, while the contracting channel involves a sequential transition. We also study the time sequence of the sequential and nonsequential transitions and find that the opposite angular distribution development is due to the different degrees of molecular alignment in these two degenerated channels.

In strong laser fields, small molecules can be rapidly aligned with the laser polarization due to the torque on the laser-induced molecular dipole moment[1–5]. Molecular alignment can be realized either adiabatically or non-adiabatically, when the laser pulse duration is longer or shorter than the rotational period of the molecule, respectively[5]. The non-adiabatic alignment by using ultrashort laser pulses is of particular interest since the aligned molecules are under field-free conditions and therefore subsequent dynamics will not be influenced by external fields[5]. Molecular alignment has been an active research topic in strong field science in the past two decades, due to its potential applications in both physics including ultrafast dynamic imaging[4,6–9], molecular tomography[10–12], and attosecond science[5,13–15], and chemistry, since most chemical reactions depend on the relative orientation of the reactants and the absorption of polarized light in photochemical processes also depends on the alignment of the molecule[2,5,10,16].

For molecular dissociative ionization, various dissociation channels following different charged states can occur due to the multiple degrees of freedom and the complex multielectron effects of molecules[17–21]. Furthermore, degenerated channels following the same charged state have also been observed in strong field-molecular interactions[22–24]. It is of great importance to study the alignment effect in these different dissociation channels of a molecule, since different dissociation channels usually lead to different end products with different kinetic energy and/or residing in different excited states[17–21]. If the end products can be differentiated or controlled by the alignment effect, it may open up a possibility to control chemical pathways simply with laser alignment effect[2,5,10,16]. Molecular alignment in dissociative ionization channels has been widely studied in the past[1–12]; however, no studies have been performed on degenerated channels from the same charge states in a molecule.

Our previous studies identified two degenerated $N^+ + N^+$ channels from N_2, a fast channel with a higher kinetic energy release (KER) and a slow channel with a lower KER[22,23,25]. In this work, we use these two channels to study, for the first time, strong-field induced molecular alignment effect in degenerated dissociation channels. When we measure the angular distribution of the dissociation fragments as increasing the laser intensity, an opposite angular distribution development is observed in these two channels, one expanding and one contracting. We identify that the expanding angular distribution comes from the fast channel involving a nonsequential transition, whereas the contracting angular distribution comes from the slow channel that involves a sequential transition. Our further study on the time sequence of the sequential and nonsequential transitions indicate that the opposite angular distribution development is due to different degrees of strong-filed induced molecular alignment in these two degenerated channels.

The Institute of Optics, University of Rochester, Rochester, New York, 14627, USA. Correspondence and requests for materials should be addressed to C.G. (email: guo@optics.rochester.edu)

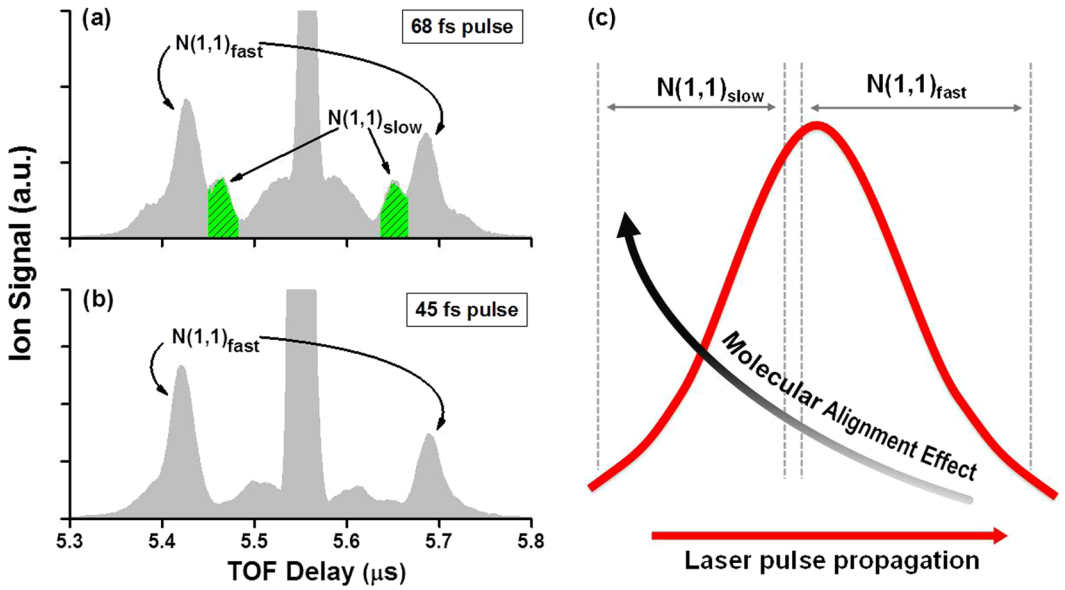

Figure 1. TOF spectra for the $N(1,1)_{fast}$ and $N(1,1)_{slow}$ channels from ionization and dissociation of N_2 using linearly polarized (**a**) 68-fs and (**b**) 45-fs pulses. $N(1,1)_{slow}$ is clearly seen in 68-fs pulses but nearly disappears in 45-fs pulses. (**c**) Schematic illustration of the formation time sequence of $N(1,1)_{fast}$ and $N(1,1)_{slow}$.

Results

Polar charts of molecular orientation distribution. The two degenerated $N^+ + N^+$ channels from double-ionization-induced dissociation of N_2 have been identified in our previous studies[22,23]: a fast $N^+ + N^+$ channel with a higher KER of 7.0 eV [labeled as $N(1,1)_{fast}$], and a slow $N^+ + N^+$ channel with a lower KER of 3.8 eV [labeled as $N(1,1)_{slow}$] (see Fig. 1(a), which shows the TOF mass spectrum of N^+ ion peaks obtained with linearly polarized 68-fs pulse at an intensity of 4×10^{14} W/cm^2). Figure 2 shows the polar charts of the measured molecular orientation distribution of $N(1,1)_{slow}$ and $N(1,1)_{fast}$ obtained with 68-fs pulses at different laser intensities, $2I_0$, $3I_0$, and $4I_0$, with $I_0 = 10^{14}$ W/cm^2. To see the change of the distribution profile, we superimpose the curve at $2I_0$ to all other curves, shown as the solid dots in Fig. 2. Distinctive difference can be seen between the two channels when the angular distribution profile develops with laser intensity. For $N(1,1)_{slow}$ [Fig. 2(b),(c) and (d)], the profile at $4I_0$ clearly gets contracted compared to the $2I_0$ guideline, which can be seen quantitatively from the $<\cos^2\theta>$ measure of alignment: 0.83 at $2I_0$ and 0.86 at $4I_0$. A contraction in the angular distribution profile with increasing intensity, i.e. an increase in the $<\cos^2\theta>$ measure, indicates that molecules are more aligned towards the laser polarization[5,6,11,26]. Therefore, as the laser intensity increases from $2I_0$ to $4I_0$, more molecules are aligned towards the laser polarization when $N(1,1)_{slow}$ is created. In contrast, for $N(1,1)_{fast}$ [Fig. 2(e),(f) and (g)], an expansion is clearly seen in the angular distribution profile when the laser intensity increases from $2I_0$ to $4I_0$, with the $<\cos^2\theta>$ measure decreasing from 0.77 to 0.73. While an expansion in the angular distribution profile with increasing intensity has not been commonly seen in previous molecular alignment studies, nor explicit mechanisms have been established[5,6], it certainly does not indicate a higher degree of alignment in this channel.

Note that an isotropic distribution across all θ corresponds to a $<\cos^2\theta>$ value of 0.33. However, due to the detection setup of the experiment, the signal measured is not across the entire space but rather is a slice of the entire spatial distribution. For this reason, an isotropic distribution gives a measure of $<\cos^2\theta>$ to be 0.5. At the low intensity end of our experiments, both $N(1,1)_{slow}$ and $N(1,1)_{fast}$ show a $<\cos^2\theta>$ value larger than 0.5 and this could be due to two possible mechanisms: the ionization rate of the channel is not angularly constant, and/or a certain degree of alignment that has been achieved when the channel is formed[5,12]. According to previous studies, the angular ionization rate of a molecular fragmentation channel, which is closely related to the molecular orbital characteristics, could significantly impact the angular distribution of fragments[6,11,12,27–29]. In the following studies, we will explore which effect plays a major role leading to the large $<\cos^2\theta>$ value in these two channels.

The relationship of the laser intensity, molecular ionization rate, and the angular distribution data. When we rotate the laser polarization and introduce an angle θ between the laser polarization and the TOF axis (i.e. the molecular axis since only ions having their velocity aligned with the TOF axis will be detected), the equivalent E-field strength along the molecular axis is $E\cos\theta$ and the equivalent laser intensity along the molecular axis is in proportion to $(E\cos\theta)^2$. When we vary the angle θ, we vary the equivalent laser intensity proportion along the molecular axis and thus vary the corresponding ion yield rate. Therefore, we fit the angular distribution data by using a $\cos^2\theta$ function with an exponential order n, i.e. $(\cos^2\theta)^n$, aiming at revealing the correlation between the intensity dependence of the angular distribution data and the intensity dependence of the ion yield rate of the channel. The fitting is shown in Fig. 3(a–d). We can see that $N(1,1)_{fast}$ is fitted by $(\cos^2\theta)^3$ at the high intensity end and $(\cos^2\theta)^4$ at the low intensity end (plus an angle-independent offset that accounts for the weak signal of $N(1,1)_{fast}$ when the laser polarization is perpendicular to the molecular axis, i.e. the components

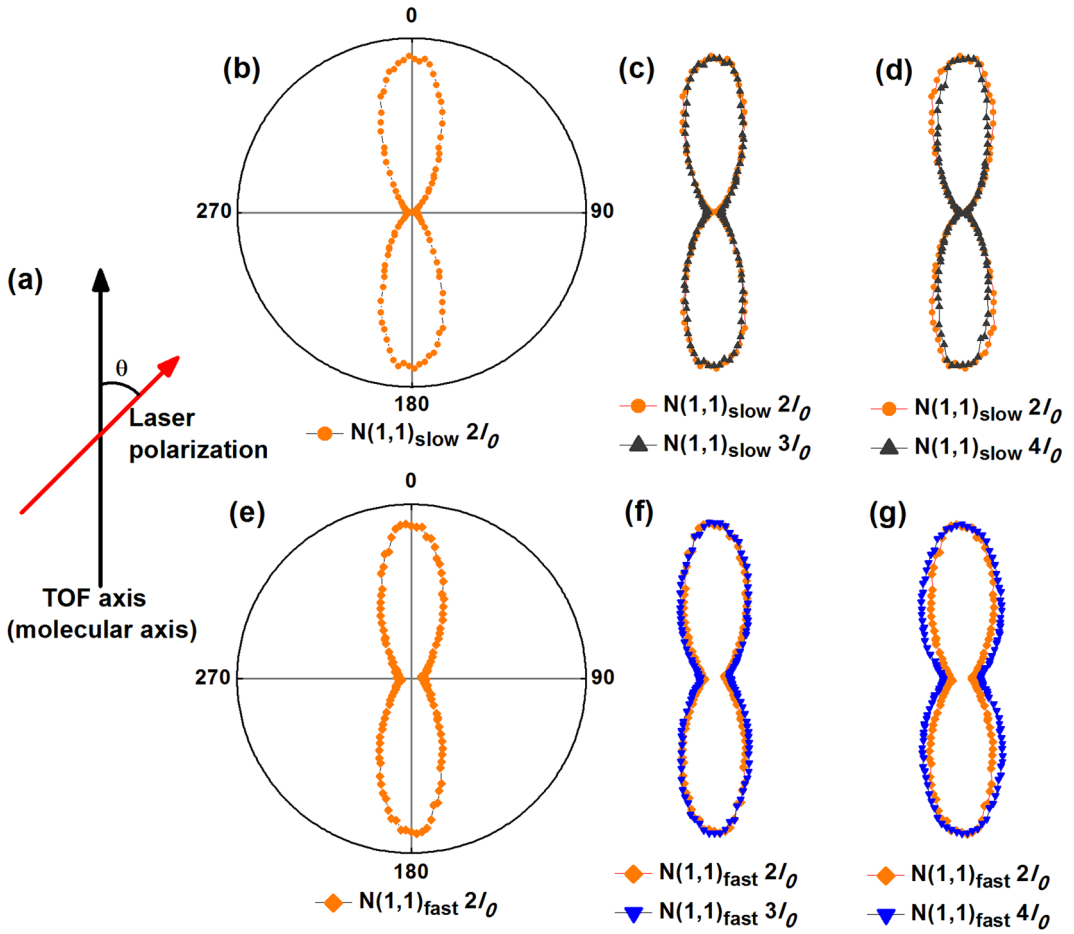

Figure 2. Polar charts of measured angular distribution of $N(1,1)_{slow}$ [(**b**–**d**)] and $N(1,1)_{fast}$ [(**e**–**g**)] at different laser intensities: $2I_0$, $3I_0$, and $4I_0$, where $I_0 = 10^{14}$ W/cm^2. The magnitude of the data points is normalized to fit the window and for easy comparison by overlapping with other distribution profile, and therefore is in arbitrary units. The profile at $2I_0$ is superimposed in each of the other profiles at $3I_0$ and $4I_0$ for each channel. The lower half of the data in each panel is mirrored from the upper half. (**a**) Illustration of the geometric configuration of the experimental setup. The TOF axis (i.e. the molecular axis) is vertical in this plane while the direction of laser polarization varies at angle θ with respect to the TOF axis in the same plane.

at $\theta = 90$ and 180 degree in Fig. 2), while $N(1,1)_{slow}$ is fitted by $(cos^2\theta)^6$ at the high intensity end and $(cos^2\theta)^5$ at the low intensity end.

Next, we compare the angular distribution data with the ionization rate of each channel obtained by ion yield curves[30,31]. We plot the ion yield curves for $N(1,1)_{slow}$ and $N(1,1)_{fast}$ as a function of laser intensity in log scale in Fig. 4. The ion yield curves are obtained with the same TOF spectrometer using linearly polarized laser beam with polarization parallel to the molecular axis. By fitting the ion yield curves of $N(1,1)_{fast}$ with an exponential function, we find that the exponential order is 3.7 and 4.4 at the intensities of $4I_0$ and $2I_0$, respectively, as marked in Fig. 4. The exponential order for $N(1,1)_{slow}$ is 2.3 and 3.1 at the high and low intensities, respectively. Note that the exponential order is smaller at the high intensity end than the low intensity end for both channels and this is due to saturation in these channels and/or depletion of this channel by higher charged states when intensity gets higher[22,31].

The fitting order of the angular distribution data at the high and low intensities, 3 and 4, coincides with the exponential order of the ion yields of $N(1,1)_{fast}$, 3.7 and 4.4, at the corresponding intensities, as shown in Fig. 4. The small discrepancy could be due to the contribution from that the perpendicular component of the laser field with respect to the molecular axis. However, this component should only play a minor role since we see a very weak signal strength of $N(1,1)_{fast}$ when the laser polarization is perpendicular to the molecular axis (i.e. the horizontal component in Fig. 2). On the other hand, the consistence between the fitting of the angular distribution data and the ion yield curves of $N(1,1)_{fast}$ indicates that the angular distribution of $N(1,1)_{fast}$ is dominantly determined by its ionization rate, or more precisely, angular ionization rate, throughout our intensity range.

In contrast, the angular distribution of $N(1,1)_{slow}$ is fitted by $(cos^2\theta)^6$ at the high intensity end and $(cos^2\theta)^5$ at the low intensity end, as shown in Fig. 3(c) and (d). The exponential fitting orders, 6 and 5, significantly diverge from the corresponding fitting orders of the ion yield curve, 2.3 and 3.1, as seen in Fig. 4. This indicates that the angular distribution profile of $N(1,1)_{slow}$ is not solely determined by its angular ionization rate; instead, there must

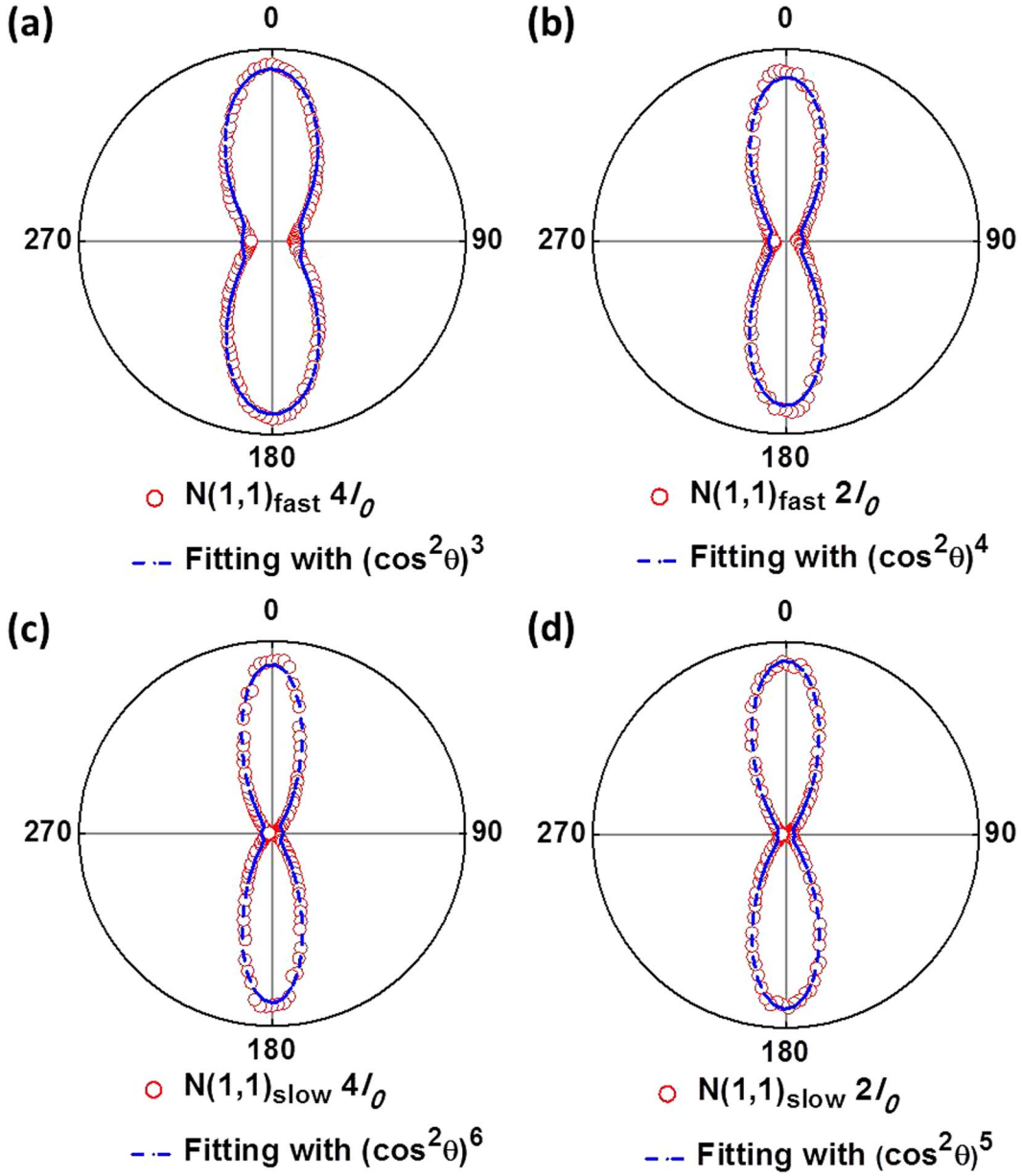

Figure 3. (**a**–**d**) Fitting of the angular distribution data with a $\cos^2\theta$ function. See text for more details.

be other mechanisms leading to the substantial divergence between the angular distribution fitting and the ionization rate fitting, which very likely is the molecular alignment effect. The fact that the fitting order of the angular distribution profile is greatly larger than the ionization rate indicates that the molecules (or the fragmented ions) are more aligned towards the laser polarization when $N(1,1)_{slow}$ is formed, resulting in a contracted distribution profile[5,6,11,26]. Furthermore, when the intensity increases from $2I_0$ to $4I_0$, the fitting order of ionization rate of $N(1,1)_{slow}$ decreases from 3.1 to 2.3. However, the fitting order of the angular distribution profile increases from 5 to 6. The greater discrepancy between the two fittings as intensity increases indicates that the alignment degree in $N(1,1)_{slow}$ is increased when intensity increases.

Formation dynamics of the degenerated dissociation channels. To understand why we observe different alignment effect in these two degenerated channels, we take a look at their formation dynamics. Our previous studies have shown that $N(1,1)_{fast}$ involves a nonsequential double ionization (NSDI) transition, where the two electrons are removed almost simultaneously when the laser intensity rises sufficiently high[25,32,33]. In contrast, $N(1,1)_{slow}$ is formed through a sequential double ionization (SDI) via enhanced ionization (EI)[23] in a two-step transition: N_2 firstly loses one electron and starts to dissociate, followed by an enhanced ionization of a second electron when the internuclear distance reaches the critical internuclear distance R_c in about 43 fs[23,34]. Therefore, $N(1,1)_{fast}$ is mostly formed at the leading edge of the 68-fs pulse, while $N(1,1)_{slow}$ is formed at the trailing edge. This is further confirmed by a time sequence study with varying pulse durations as shown in Fig. 1(a) and (b).

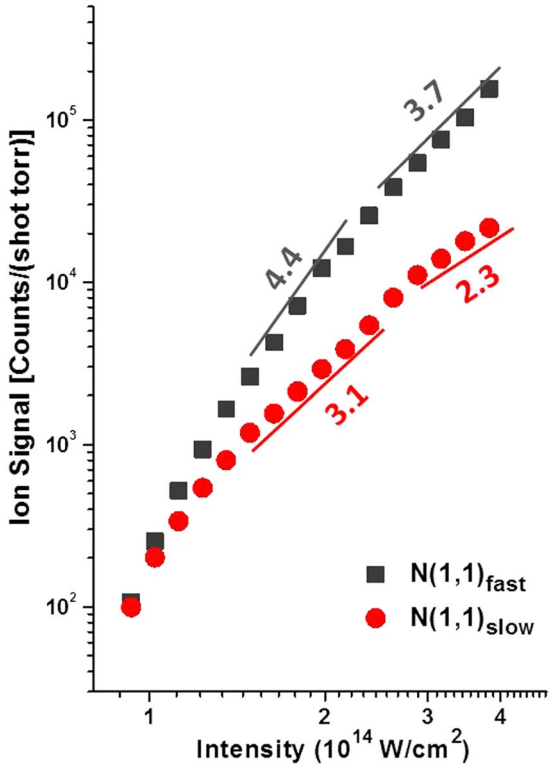

Figure 4. Fitting with the exponential order of the ion yield curves for $N(1,1)_{fast}$ and $N(1,1)_{slow}$ at the intensity corresponding to $2I_0$ and $4I_0$, where $I_0 = 10^{14}$ W/cm^2.

Figure 1(a) shows the TOF spectrum of N^+ obtained with a longer 68-fs pulse and 4(b) with a shorter 45-fs pulse. We can see that the $N(1,1)_{slow}$ peaks nearly disappear in the shorter 45-fs pulses and that is because the pulse duration is insufficient for this channel to form; in contrast, $N(1,1)_{fast}$ consistently presents in both 45 and 68-fs pulses, indicating that this channel is formed at the pulse leading edge. A schematic of the formation time sequence of $N(1,1)_{slow}$ and $N(1,1)_{fast}$ is shown in Fig. 1(c).

Discussion

Previous studies have shown that molecular alignment can be achieved in as fast as tens of femtoseconds for small molecules exposed to intense laser fields[5,7,8]. For example, when N_2 is exposed in 45-fs pulse with a peak intensity of 1.4×10^{14} W/cm^2, the highest degree of alignment happens at 67 fs follows the aligning pulse[8]. If an event happens in a similar time scale, it will strongly experience the molecular alignment effect. Since the SDI channel $N(1,1)_{slow}$ is formed at the trailing edge of the laser pulse in about tens of fs[23,34], similar to the alignment time scale of N_2, $N(1,1)_{slow}$ will strongly experience an alignment effect (and possibly some post ionization alignment effect[12]), i.e. the molecules (or molecular ions) that form $N(1,1)_{slow}$ experience stronger alignment and therefore a higher degree of alignment is seen in its angular distribution. As the laser intensity increases, laser field-induced alignment becomes stronger[5,6,8,9,11,35], and this leads to the contraction as we see in the angular distribution of $N(1,1)_{slow}$ in Fig. 2.

In contrast, the NSDI channel $N(1,1)_{fast}$ is formed at the leading edge of the laser pulse, where both electrons are almost simultaneously removed as fast as the laser intensity rises sufficiently high[25,32,33], followed by strong Coulomb explosion and molecular bond breaking. Therefore, the NSDI channel only experiences limited alignment effect and/or post ionization alignment[12]. As a result, the angular distribution of $N(1,1)_{fast}$ is less affected by molecular alignment effect, instead, is dominantly determined by its intensity-dependent ionization rate, which leads to the coincidental fitting between the angular ion distribution data and the ionization rate curve as discussed above.

Note that in our current experimental setup we could not exclude the possibility of the post-ionization alignment effect contributing to our experimental results besides the molecular alignment effect. Some thoughts to investigate the relative strength of the post-ionization alignment effect in the SDI channel $N(1,1)_{slow}$ are provided here for future studies: a pump-probe experiment consisting of pump pulse duration being long enough for molecular alignment effect to take place but less than the critical time to trigger the SDI $N(1,1)_{slow}$ channel (e.g. 45 fs, which was reported to well align N_2 molecules [8] but insufficient to produce $N(1,1)_{slow}$ [23]), and probe pulse duration being much shorter (e.g. a few fs) to trigger the SDI $N(1,1)_{slow}$ channel at the critical nuclear distance, R_c. The angular distribution of the SDI $N(1,1)_{slow}$ channel from this pump-probe experiment, if compared with single- long-pulse experiment results (e.g. the results shown in this paper), could reveal the relative strength of the post-ionization alignment effect. Here we note on the relative strength and that is because the parental state of the $N(1,1)_{slow}$ channel, i.e. the N_2^+ state, may involve both the molecular alignment and the post-ionization

alignment effects since single ionization of N_2 could happen immediately once the pump pulse arrives and therefore it may not be easy to completely exclude post-ionization alignment effect in the N_2^+ state.

In summary, we perform a study on the strong-field molecular alignment effect in two degenerated channels from double ionization-induced dissociation of N_2. Our previous study identified two $N^+ + N^+$ states, a fast channel with a higher KER and a slow channel with a lower KER; the fast channel is a nonsequential channel and the slow is a sequential channel. By measuring the angular distribution of dissociation fragments, we observe opposite angular distribution development in these two channels as the laser intensity increases, one expanding and one contracting. Our further study shows that the expanding angular distribution comes from the nonsequential channel, whereas the contracting angular distribution comes from the sequential channel. A further analysis of the time sequence of the sequential and nonsequential transitions reveals that the opposite angular distribution development is due to different degrees of strong-field induced molecular alignment in these two degenerated channels.

Methods

Ion detection and collection is realized with a recently modified time-of-flight (TOF) spectrometer[22,23]. The chamber base pressure is less than 5.0×10^{-10} Torr. We measure the molecular orientation distribution by using our TOF spectrometer. The 2.5-mm pinhole opening on the voltage plates in our TOF spectrometer ensures that only ions having their velocity aligned with the TOF axis will be detected. A half-wave plate (HWP) is used before the focusing lens to control the angle of the laser polarization with respect to the TOF axis. Ion signal of a specific channel is collected as we rotate the HWP, which is equivalent to a scanning of the angular distribution of this channel. Figure 2(a) illustrates the geometric configuration of the experimental setup.

The laser used is a Ti:sapphire system consisting of a regenerative amplifier and a multi-pass amplifier that delivers pulses of 1.0–1.2 mJ/pulse at a 1 kHz repetition rate with the central wavelength at 800 nm. By adjusting the bandwidth of the seed pulse, 25 and 50 nm used in this work, before entering the regenerative amplifier, we manage to generate two pulse durations at 45 and 68 fs, respectively. To minimize the chirp of both pulses, we carefully tune the stretcher and compressor while monitoring the second and third order dispersion with a home-built FROG-like spectrum and phase detection system. This approach allows us to minimize the second and third order dispersion (higher order dispersion may still exist) and therefore achieve the closest-to transform-limited pulses.

References

1. Larsen, J. J., Sakai, H., Safvan, C. P., Wendt-Larsen, I. & Stapelfeldt, H. Aligning molecules with intense nonresonant laser fields. *J Chem Phys* **111**, 7774–7781, doi:10.1063/1.480112 (1999).
2. Vrakking, M. J. J. & Stolte, S. Coherent control of molecular orientation. *Chemical Physics Letters* **271**, 209–215, doi:10.1016/s0009-2614(97)00436-3 (1997).
3. Ellert, C. & Corkum, P. B. Disentangling molecular alignment and enhanced ionization in intense laser fields. *Phys Rev A* **59**, R3170–R3173, doi:10.1103/PhysRevA.59.R3170 (1999).
4. Rosca-Pruna, F. & Vrakking, M. Experimental observation of revival structures in picosecond laser-induced alignment of I 2. *Physical Review Letters* **87**, 153902, doi:10.1103/PhysRevLett.87.153902 (2001).
5. Stapelfeldt, H. & Seideman, T. Colloquium: Aligning molecules with strong laser pulses. *Rev Mod Phys* **75**, 543–557, doi:10.1103/RevModPhys.75.543 (2003).
6. Voss, S. *et al.* High resolution kinetic energy release spectra and angular distributions from double ionization of nitrogen and oxygen by short laser pulses. *J Phys B-at Mol Opt* **37**, 4239–4257, doi:10.1088/0953-4075/37/21/002 (2004).
7. De, S. *et al.* Field-Free Orientation of CO Molecules by Femtosecond Two-Color Laser Fields. *Physical Review Letters* **103**, Artn 153002, doi:10.1103/Physrevlett.103.153002 (2009).
8. Dooley, P. W. *et al.* Direct imaging of rotational wave-packet dynamics of diatomic molecules. *Phys Rev A* **68**, 023406, doi:10.1103/PhysRevA.68.023406 (2003).
9. Muramatsu, M., Hita, M., Minemoto, S. & Sakai, H. Field-free molecular orientation by an intense nonresonant two-color laser field with a slow turn on and rapid turn off. *Phys Rev A* **79**, 011403, doi:10.1103/PhysRevA.79.011403 (2009).
10. Itatani, J. *et al.* Tomographic imaging of molecular orbitals. *Nature* **432**, 867–871, doi:10.1038/nature03183 (2004).
11. Alnaser, A. *et al.* Effects of orbital symmetries in dissociative ionization of molecules by few-cycle laser pulses. *Phys Rev A* **71**, Artn 031403, doi:10.1103/Physreva.71.031403 (2005).
12. Tong, X. M. *et al.* Post ionization alignment of the fragmentation of molecules in an ultrashort intense laser field. *J Phys B-at Mol Opt* **38**, 333–341, doi:10.1088/0953-4075/38/4/002 (2005).
13. Hentschel, M. *et al.* Attosecond metrology. *Nature* **414**, 509–513, doi:10.1038/35107000 (2001).
14. Corkum, P. B. & Krausz, F. Attosecond science. *Nat Phys* **3**, 381–387, doi:10.1038/Nphys620 (2007).
15. Krausz, F. & Ivanov, M. Attosecond physics. *Rev Mod Phys* **81**, 163–234, doi:10.1103/RevModPhys.81.163 (2009).
16. Viftrup, S. S. *et al.* Holding and Spinning Molecules in Space. *Physical Review Letters* **99**, 143602, doi:10.1103/PhysRevLett.99.143602 (2007).
17. Boyer, K., Luk, T. S., Solem, J. C. & Rhodes, C. K. Kinetic-Energy Distributions of Ionic Fragments Produced by Subpicosecond Multiphoton Ionization of N-2. *Phys Rev A* **39**, 1186–1192, doi:10.1103/PhysRevA.39.1186 (1989).
18. Guo, C., Li, M. & Gibson, G. Charge asymmetric dissociation induced by sequential and nonsequential strong field ionization. *Physical Review Letters* **82**, 2492–2495, doi:10.1103/PhysRevLett.82.2492 (1999).
19. Bandrauk, A. D. *Molecules in Laser Fields* (Marcel Dekker, 1994).
20. Guo, C., Li, M., Nibarger, J. & Gibson, G. Single and double ionization of diatomic molecules in strong laser fields. *Phys Rev A* **58**, R4271–R4274, doi:10.1103/PhysRevA.58.R4271 (1998).
21. Guo, C. Multielectron effects on single-electron strong field ionization. *Physical Review Letters* **85**, 2276–2279, doi:10.1103/PhysRevLett.85.2276 (2000).
22. Lai, W., Pei, L. & Guo, C. Dissociation of doubly and triply charged N_{2} in strong laser fields. *Phys Rev A* **84**, 043413, doi:10.1103/PhysRevA.84.043413 (2011).
23. Lai, W. & Guo, C. Direct detection of enhanced ionization in CO and N2 in strong fields. *Phys Rev A* **90**, 031401(R), doi:10.1103/PhysRevA.90.031401 (2014).
24. Wu, J., Zeng, H. & Guo, C. Non-sequential double ionization in slow charge fragmentation of doubly ionized NO. *J Phys B-at Mol Opt* **39**, 3849–3854, doi:10.1088/0953-4075/39/18/014 (2006).

25. Guo, C., Li, M., Nibarger, J. P. & Gibson, G. N. Nonsequential double ionization of molecular fragments. *Phys Rev A* **61**, art. no.-033413 (2000).
26. Gaire, B. *et al*. Laser-induced multiple ionization of molecular ion beams: N_{2}^{+}, CO^{+}, NO^{+}, and O_{2}^{+}. *Phys Rev A* **79**, 063414, doi:10.1103/PhysRevA.79.063414 (2009).
27. Pavicic, D., Lee, K. F., Rayner, D. M., Corkum, P. B. & Villeneuve, D. M. Direct measurement of the angular dependence of ionization for N-2, O-2, and CO_2 in intense laser fields. *Physical Review Letters* **98**, Artn 243001, doi:10.1103/Physrevlett.98.243001 (2007).
28. Lin, C. D., Tong, X. M. & Zhao, Z. X. Effects of orbital symmetries on the ionization rates of aligned molecules by short intense laser pulses. *J Mod Optic* **53**, 21–33, doi:10.1080/09500340500159492 (2006).
29. Alnaser, A. S. *et al*. Effects Of Molecular Structure on Ion Disintegration Patterns In Ionization of ${\mathrm{O}}_{\mathrm{2}}$ and ${\mathrm{N}}_{\mathrm{2}}$ by Short Laser Pulses. *Physical Review Letters* **93**, 113003, doi:10.1103/PhysRevLett.93.113003 (2004).
30. Ammosov, M., Delone, N. B. & Krainov, V. P. Tunnel ionization of complex atoms and of atomic ions in an alternating electromagnetic field. *Sov. Phys. JETP* **64**, 1191–1194 (1986).
31. Guo, C., Li, M., Nibarger, J. P. & Gibson, G. N. Single and double ionization of diatomic molecules in strong laser fields. *Phys Rev A* **58**, R4271–R4274, doi:10.1103/PhysRevA.58.R4271 (1998).
32. Fittinghoff, D. N., Bolton, P. R., Chang, B. & Kulander, K. C. Observation of Nonsequential Double Ionization of Helium with Optical Tunneling. *Physical Review Letters* **69**, 2642–2645, doi:10.1103/PhysRevLett.69.2642 (1992).
33. Corkum, P. B. Plasma perspective on strong field multiphoton ionization. *Physical Review Letters* **71**, 1994–1997, doi:10.1103/PhysRevLett.71.1994 (1993).
34. Chelkowski, S. & Bandrauk, A. D. Two-step Coulomb explosions of diatoms in intense laser fields. *Journal of Physics B: Atomic, Molecular and Optical Physics* **28**, L723–L731, doi:10.1088/0953-4075/28/23/004 (1995).
35. Kanai, T. & Sakai, H. Numerical simulations of molecular orientation using strong, nonresonant, two-color laser fields. *The Journal of Chemical Physics* **115**, 5492–5497, doi:10.1063/1.1398311 (2001).

Acknowledgements

This research was supported by the Air Force Office of Scientific Research (USA) and Bill & Melinda Gates Foundation.

Author Contributions

W. Lai, A. Heins, and C. Guo conceived and designed the experiments; W. Lai performed the experiments and analyzed the data.

Additional Information

Competing Interests: The authors declare that they have no competing interests.

Publisher's note: Springer Nature remains neutral with regard to jurisdictional claims in published maps and institutional affiliations.